Highlights

Efficient implementation of a new formula for the complex scaled resolvent of the Helmholtz equation in inhomogeneous media

Kiril Datchev,Shingyu Leung,Jianliang Qian,Yuxiao Wei

- Explicit representation of the complex scaled resolvent of the Helmholtz equation in an inhomogeneous medium.
- Incorporation of a Hadamard–Babich–ansatz-based asymptotic resolvent into a gluing framework to construct the resolvent for the complex scaling method.
- Efficient implementation based on multivariate low-rank representation.

Efficient implementation of a new formula for the complex scaled resolvent of the Helmholtz equation in inhomogeneous media*

Kiril Datchev[a], Shingyu Leung[b], Jianliang Qian[c,*] and Yuxiao Wei[b]

[a]Department of Mathematics, Purdue University, West Lafayette, IN 47907, USA
[b]Department of Mathematics, The Hong Kong University of Science and Technology, Clear Water Bay, Hong Kong
[c]Departments of Mathematics and CMSE, Michigan State University, East Lansing, MI 48824, USA

ARTICLE INFO

Keywords:
Helmholtz equation
Complex scaling
Perfectly matched layer
Green's function
Hadamard-Babich ansatz

ABSTRACT

In this paper, we develop an explicit representation of the complex scaled resolvent of the Helmholtz equation in an inhomogeneous medium. We surround the computational domain with a complex scaling layer of a constant thickness and a homogeneous (constant) property (also known as a perfectly matched layer, or PML), and employ suitable cutoff functions to smoothly glue the complex-scaled resolvent in the homogeneous medium with the unscaled resolvent in the inhomogeneous medium, where the latter is given by the Green's function expressed via the Hadamard-Babich ansatz. The resulting resolvent possesses the following unique features: on the one hand, it acts on the source term through integration and is thus free from numerical dispersion error, allowing the number of grid points per dimension to scale linearly with frequency; on the other hand, it provides an explicit representation of the Green's function for the complex-scaled Helmholtz equation in an inhomogeneous medium in the form of a geometric series, which holds significant potential for applications in scattering problems. Two-dimensional numerical examples demonstrate the convergence and performance of the proposed resolvent.

1. Introduction

The complex scaling method, also known as the perfectly matched layer (PML) method, plays an important role in the theory of scattering resonances [26, 8] as well as in the numerical simulation of a wide range of unbounded wave fields[4]. By surrounding the original computational domain with a region where a complex coordinate transformation is applied, outgoing waves are absorbed without reflection and decay exponentially. Thus, on the outer boundary of this layer, a homogeneous Dirichlet or Neumann condition can be naturally imposed. As a result, the complex scaling method for the Helmholtz equation can be solved using finite-difference frequency-domain (FDFD) or finite element methods. However, when applied to high-frequency wave fields, these direct methods may suffer from dispersion or pollution errors [3, 2], which require extremely fine computational grids (or large numbers of degrees of freedom) to resolve the oscillations, making them prohibitively expensive in practice.

Therefore, alternative methods have been sought to resolve these highly oscillatory wave phenomena. The solution to the Helmholtz equation can be obtained by applying the resolvent operator to the source term, which is typically realized through a volume integral involving the Green's function. The Green's function for the Helmholtz equation in homogeneous media is well known. For the complex scaling method, the corresponding Green's function has been defined by analytic extension in [12] and successfully employed in boundary integral equations [18] for scattering problems. In inhomogeneous media, the Green's function generally lacks an analytical representation. To overcome this difficulty, asymptotic representations inspired by geometrical optics—such as the WKBJ ansatz and the Hadamard-Babich ansatz[1]—have been proposed and used in a range of high-frequency problems[19, 17, 15]. However, the amplitude and phase functions in these asymptotic solutions must be obtained sequentially by solving the eikonal and transport equations, and unlike in the homogeneous case, they cannot directly yield a solution to the complex scaling method via analytic continuation. This motivates us to seek alternative representations of the resolvent in inhomogeneous media, which have broad applications in scattering problems.

Inspired by [7], we construct the complex scaled resolvent $R_\sigma(\omega)$ in inhomogeneous media by gluing together the complex scaled resolvent $R_{\sigma,0}(\omega)$ in homogeneous media and the resolvent $R(\omega)$ without complex scaling in inhomogeneous media. Here, ω denotes the angular frequency and σ is an auxiliary function required for complex

*Corresponding author
kdatchev@purdue.edu (K. Datchev); masyleung@ust.hk (S. Leung); jqian@msu.edu (J. Qian); weiyuxiao@ust.hk (Y. Wei)

scaling. The resolvent $R_{\sigma,0}(\omega)$ has been studied in [12] and applied to scattering problems [18], and its explicit representation can be obtained by performing analytic continuation on the distance function and the free-space Green's function. Regarding the resolvent $R_\sigma(\omega)$, or equivalently the Green's function in an inhomogeneous medium, we adopt the the Hadamard–Babich (HB) ansatz as the building block, since, unlike the usual geometric optics methods, it provides an asymptotic representation that remains uniformly accurate near the point source. After precomputing some HB ingredients and developing multivariate Chebyshev representations of these ingredients, the numerical HB ansatz can provide the asymptotic Green's function at each source-target pair at an $O(1)$ computational cost per evaluation, which forms the basis for the design of fast algorithms.

The resulting resolvent $R_\sigma(\omega)$ can be represented as a geometric series whose expansion factor decays faster than any polynomial in $\frac{1}{\omega}$, leading to rapid convergence when ω is large. The application of $R_\sigma(\omega)$ is implemented through a successive application of several integral kernels associated with different Green's functions. Although in this paper, we simply construct these oscillatory kernels explicitly via Chebyshev interpolation and apply them using matrix–vector multiplications to demonstrate the accuracy of the proposed method, we remark that we have already developed a series of works that use the butterfly algorithm to accelerate constructing and applying such Green's function kernels [19, 22, 23, 17, 27, 28, 15]. The application of the resolvent equipped with these techniques to scattering problems constitutes a part of our ongoing work.

2. Complex scaling

Let $\nu,\ \rho:\ \mathbb{R}^m \to (0,\infty)$ be analytic functions which are bounded above and below by positive constants, and which are equal to 1 outside of a compact rectangle $K \subset \mathbb{R}^m$. Let

$$P = -\rho^{-1}\nabla\cdot(\nu\nabla), \qquad P:\ \mathcal{D}\to\mathcal{H},$$

where $\mathcal{H} = L^2(\mathbb{R}^m;\rho\,dx)$ and $\mathcal{D} = \{u\in\mathcal{H}:\ Pu\in\mathcal{H}\}$. Then we define the Helmholtz equation as

$$(P-\omega^2)u = -\rho^{-1}\nabla\cdot(\nu\nabla u) - \omega^2 u = f,\ \boldsymbol{x}\in\mathbb{R}^m, \tag{2.1}$$

where ω denotes the angular frequency, $f\in L^2(\mathbb{R}^m)$ is the source term with compact support in K, and u obeys the Sommerfeld radiation condition at infinity. Specifically, choosing $f=\delta(\boldsymbol{x}_0)$ in (2.1), we obtain the Green's function $G\left(\omega,\boldsymbol{x}_0;\boldsymbol{x}\right)$ excited at $\boldsymbol{x}_0$.

The resolvent $(P-\omega^2)^{-1}:\ \mathcal{H}\to\mathcal{D}$ is defined for $\operatorname{Im}\omega>0$, because P is a non-negative self-adjoint operator. Then for $\omega>0$ the limit

$$R(\omega)f = \lim_{\varepsilon\to 0^+}(P-(\omega+\mathrm{i}\varepsilon)^2)^{-1}f$$

exists and obeys the Sommerfeld radiation condition at infinity [8, Section 4.4]. We remark that the action of the resolvent operator $R(\omega)$ can be implemented as a volume integral involving the Green's function $G\left(\omega,\boldsymbol{x}_0;\boldsymbol{x}\right)$, namely

$$\Big[R(\omega)f\Big](\boldsymbol{x}_0) = \int_{\mathbb{R}^m} G\left(\omega,\boldsymbol{x}_0;\boldsymbol{x}\right) f(\boldsymbol{x})\,\mathrm{d}\boldsymbol{x}. \tag{2.2}$$

For example, if ν and ρ are identically 1 and $m=3$, then

$$\Big[R(\omega)f\Big](\boldsymbol{x}_0) = \frac{1}{4\pi}\int_{\mathbb{R}^3}\frac{e^{\mathrm{i}\omega|\boldsymbol{x}_0-\boldsymbol{x}|}}{|\boldsymbol{x}_0-\boldsymbol{x}|}f(\boldsymbol{x})\,\mathrm{d}\boldsymbol{x}.$$

To truncate equation (2.1) onto a bounded domain Ω that contains K, we now define the complex scaling operator [26], also known as a perfectly matched layer operator [4], as follows. Let $\sigma_1,\dots,\sigma_m:\ \mathbb{R}\to[0,\infty)$ be smooth functions, such that the product $\sigma_1(x_1)\cdots\sigma_m(x_m)$ equals 0 inside Ω, and such that each σ_j is a positive constant outside of a compact set Ω_P that contains Ω. We introduce a complex stretching of the coordinates with:

$$\widetilde{x}_j\left(x_j\right) = x_j + \mathrm{i}\int_0^{x_j}\sigma_j(t)dt, \tag{2.3}$$

and define

$$\partial_{x_j,\sigma_j} = \frac{1}{1+\mathrm{i}\sigma_j(x_j)}\partial_{x_j}, \qquad \nabla_\sigma = (\partial_{x_1,\sigma_1}, \dots, \partial_{x_m,\sigma_m}),$$

and the complex scaled resolvents in inhomogeneous and homogeneous media are, respectively,

$$R_\sigma(\omega) = (-\rho^{-1}\nabla_\sigma \cdot (\nu\nabla_\sigma) - \omega^2)^{-1}, \qquad R_{\sigma,0}(\omega) = (-\nabla_\sigma \cdot \nabla_\sigma - \omega^2)^{-1}.$$

By standard results in complex scaling/PML [8, Section 4.5], these resolvents are defined for $\omega > 0$, acting on $f \in L^2(\mathbb{R}^m)$, without any need to take a limit, or to impose a support or decay condition on f.

The complex scaled resolvent $R_{\sigma,0}(\omega)$ in a homogeneous medium admits an explicit representation, which can be obtained via analytic continuation of the Green's function in the homogeneous medium, dubbed the PML-transformed free-space Green's function[12]:

$$\widetilde{G}(\omega, \boldsymbol{x}_0; \boldsymbol{x}) = G\left(\omega, \widetilde{\boldsymbol{x}}_0; \widetilde{\boldsymbol{x}}\right) = \begin{cases} \frac{\mathrm{i}}{4} H_0^{(1)}(\omega\tilde{r}(\widetilde{\boldsymbol{x}}_0, \widetilde{\boldsymbol{x}})), & m = 2, \\ \frac{\exp(\mathrm{i}\omega\tilde{r}(\widetilde{\boldsymbol{x}}_0,\widetilde{\boldsymbol{x}}))}{4\pi\tilde{r}(\widetilde{\boldsymbol{x}}_0,\widetilde{\boldsymbol{x}})}, & m = 3, \end{cases} \tag{2.4}$$

where $\tilde{r}$ is the complex distance function given by

$$\tilde{r}(\widetilde{\boldsymbol{x}}_0, \widetilde{\boldsymbol{x}}) = \left(\sum_{j=1}^{m} \left(\widetilde{x}_{0,j} - \widetilde{x}_j\right)^2\right)^{1/2}, \tag{2.5}$$

and the half-power operator $z^{1/2}$ is chosen to be the branch of $\sqrt{z}$ with nonnegative real part for $z \in \mathbb{C}\backslash(-\infty, 0]$ such that $\arg\sqrt{z} \in \left(-\frac{\pi}{2}, \frac{\pi}{2}\right]$.

3. Main result

Suppose the resolvent operator $R(\omega)$ under consideration is polynomially bounded in the sense that there is N such that for any $\chi \in C_c^\infty(\mathbb{R}^m)$ we have

$$\|\chi R(\omega)\chi\|_{L^2(\mathbb{R}^m)\to H^1(\mathbb{R}^m)} = O(\omega^N), \tag{3.1}$$

as $\omega \to \infty$. For example, if the problem is nontrapping, then (3.1) holds with $N = 0$ by [8, (6.2.22)]. As in [8, (6.2.21)], we similarly have

$$\|R_{\sigma,0}(\omega)\|_{L^2(\mathbb{R}^m)\to H^1(\mathbb{R}^m)} = O(1).$$

The following is an application of the main theorem of [7].

Theorem 1. *For $\omega \gg 1$, there is a formula for the resolvent $R_\sigma(\omega)$ in terms of the resolvent $R_{\sigma,0}(\omega)$ and the cutoff resolvent $\chi R(\omega)\chi$, for suitable $\chi \in C_c^\infty(\mathbb{R}^m)$. It is given in formula (3.3) below.*

Proof 1. *Let χ_K, χ_∞, $\tilde{\chi}_K$, and $\tilde{\chi}_\infty$ be smooth cutoff functions, with the following properties:*

a) $\chi_K + \chi_\infty = 1$,

b) $\tilde{\chi}_K = 1$ near the support of χ_K, and $\tilde{\chi}_\infty = 1$ near the support of χ_∞,

c) $\tilde{\chi}_\infty = 0$ near K, and $\tilde{\chi}_K = 0$ near the set where any $\sigma(x_j)$ $(j = 1, 2, \cdots, m)$ is nonzero,

d) χ_K factors as a product of functions of one variable $\chi_K(x) = \chi_{K,1}(x_1)\cdots\chi_{K,m}(x_m)$, and so does each of the other three cutoffs.

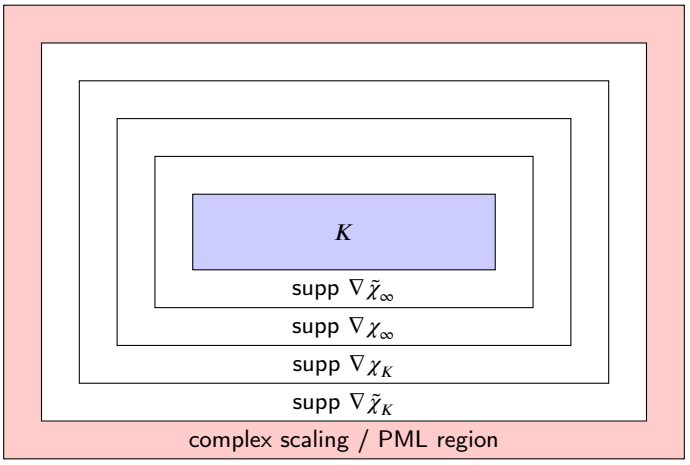

Figure 1: The cutoffs used to construct the resolvent. In the white region, where all derivatives of all cutoffs are supported, we have $\nu(x) = \rho(x) = 1$ and $\sigma_j(x_j) = 0$ for all j. The complex scaling / PML region contains $\partial\Omega$ and $\partial\Omega_P$.

Thus χ_K and $\tilde{\chi}_K$ are cutting off near K, while χ_∞ and $\tilde{\chi}_\infty$ are cutting off near the set where we put complex scaling/PML. See Figure 1.

Then define

$$F = \tilde{\chi}_K R(\omega)\chi_K + \tilde{\chi}_\infty R_{\sigma,0}(\omega)\chi_\infty.$$

We compute

$$(P_\sigma - \omega^2)F = I + A_K + A_\infty, \quad \text{where} \quad A_K = [\tilde{\chi}_K, \Delta]R(\omega)\chi_K, \quad A_\infty = [\tilde{\chi}_\infty, \Delta]R_{\sigma,0}(\omega)\chi_\infty.$$

Here we have used the commutator relation defined by $[\tilde{\chi}_K, \Delta] = \tilde{\chi}_K\,\Delta - \Delta\,\tilde{\chi}_K$. Note that $A_K^2 = A_\infty^2 = 0$. By [7, (3.3)], for any N we have

$$\|A_\infty A_K\|_{L^2(\mathbb{R}^m)\to H^N(\mathbb{R}^m)} = O(\omega^{-N}). \tag{3.2}$$

This, together with the identity

$$(P_\sigma - \omega^2)F(I - A_K - A_\infty + A_K A_\infty) = I - A_\infty A_K + A_\infty A_K A_\infty,$$

implies that

$$R_\sigma(\omega) = F(I - A_K - A_\infty + A_K A_\infty)\sum_{j=0}^{\infty}(A_\infty A_K - A_\infty A_K A_\infty)^j, \tag{3.3}$$

with the geometric series converging for $\omega \gg 1$ thanks to (3.2).

We note that for $\omega \gg 1$, estimate (3.2) ensures that the norm of $A_\infty A_K - A_\infty A_K A_\infty$ is sufficiently small, so that retaining only the leading term in the series is typically sufficient.

In fact, for the source term f compactly supported in K, we have

$$\chi_\infty f = 0, \ \chi_K f = f. \tag{3.4}$$

Thus

$$A_\infty f = [\tilde{\chi}_\infty, \Delta]R_{\sigma,0}(\omega)\chi_\infty f = 0. \tag{3.5}$$

Applying the leading-term truncation of (3.3) to f, we obtain

$$\begin{aligned} R_\sigma(\omega)f &\approx F(I - A_K - A_\infty + A_K A_\infty)f \\ &= F(I - A_K)f \\ &= \tilde{\chi}_K R(\omega)\chi_K f - \tilde{\chi}_K R(\omega)\chi_K A_K f - \tilde{\chi}_\infty R_{\sigma,0}(\omega)\chi_\infty A_K f \\ &= \tilde{\chi}_K R(\omega)\chi_K f - \tilde{\chi}_\infty R_{\sigma,0}(\omega)\chi_\infty A_K f \\ &= \tilde{\chi}_K R(\omega)f - \tilde{\chi}_\infty R_{\sigma,0}(\omega)\chi_\infty A_K f. \end{aligned} \tag{3.6}$$

Here we have used the fact that the support of

$$A_K f = [\tilde{\chi}_K, \Delta]R(\omega)\chi_K f \tag{3.7}$$

is contained in the support of the gradient of $\tilde{\chi}_K$, which is disjoint from the support of χ_K.

4. Hadamard-Babich ansatz and resolvent R_σ

The resolvent $R(\omega)$ takes the following form:

$$\Big[R(\omega)f\Big](\boldsymbol{x}_0) = \int_{\mathbb{R}^m} G\left(\omega, \boldsymbol{x}_0; \boldsymbol{x}\right) f(\boldsymbol{x})\,\mathrm{d}\boldsymbol{x}, \tag{4.1}$$

where G represents the Green's function in an inhomogeneous medium. To construct an asymptotic approximation of the Green's function, we assume that any two points within the computational domain that we are interested in are connected by a unique geodesic; consequently, we can use the Hadamard-Babich method [1, 17] to obtain the following Hankel-based ansatz so as to expand the solution $u(\boldsymbol{x}) = G(\omega, \boldsymbol{x}_0; \boldsymbol{x})$,

$$G_B\left(\omega, \boldsymbol{x}_0; \boldsymbol{x}\right) = \sum_{s=0}^{\infty} v_s\left(\boldsymbol{x}_0; \boldsymbol{x}\right) f_{s-(m-2)/2}(\omega, \tau), \tag{4.2}$$

where

$$f_q(\omega, \tau) = \mathrm{i}\frac{\sqrt{\pi}}{2} e^{iq\pi}\left(\frac{2\tau}{\omega}\right)^q \mathrm{H}_q^{(1)}(\omega\tau). \tag{4.3}$$

Here $\mathrm{H}_q^{(1)}$ is the q-th Hankel function of the first kind, the phase τ satisfies

$$4v_0\tau^2\left(\nu|\nabla\tau|^2 - \rho\right) = 0, \quad \tau(\boldsymbol{x}_0; \boldsymbol{x})|_{\boldsymbol{x}=\boldsymbol{x}_0} = 0. \tag{4.4}$$

This is equivalent to the eikonal equation,

$$|\nabla\tau| = n, \quad \tau(\boldsymbol{x}_0; \boldsymbol{x})|_{\boldsymbol{x}=\boldsymbol{x}_0} = 0, \tag{4.5}$$

when we define the slowness $n = \sqrt{\frac{\rho}{\nu}}$.

For $s \geq 0$, the coefficients v_{s+1} satisfy the recurrent system

$$4\nu\tau\nabla\tau\cdot\nabla v_{s+1} + v_{s+1}[2(2s+2-m)\rho + 2\nabla\cdot(\nu\tau\nabla\tau)] = \nabla\cdot\left(\nu\nabla v_s\right) \tag{4.6}$$

with $v_{-1} \equiv 0$ and

$$v_0\left(\boldsymbol{x}_0; \boldsymbol{x}\right)\Big|_{\boldsymbol{x}=\boldsymbol{x}_0} = \frac{n_0^m}{2\pi^{(m-1)/2}}, \quad n_0 = n\left(\boldsymbol{x}_0\right). \tag{4.7}$$

We call the above ansatz the Hadamard-Babich ansatz. The coefficients v_s, called HB coefficients, differ from the amplitude functions in classical geometrical optics such as the WKBJ method. The Hadamard–Babich ansatz absorbs

the point source singularity into the Hankel basis functions, resulting in HB coefficients that remain non-singular at the source. Consequently, this ansatz provides a uniformly accurate asymptotic solution near the point source [25].

Similar to usual geometric optics series, the Hadamard–Babich ansatz fails to capture caustics, which frequently arise in wave propagation through inhomogeneous media. This failure is primarily due to the requirement that τ^2 remains smooth, a condition that breaks down at caustics. Since this work focuses on the construction of the complex scaled resolvent, we make the simplifying assumption that the functions τ^2 and $v_s, s = 0, 1, 2, \ldots$ are analytic throughout the computational domain and for any point source position, which is a reasonable assumption in the caustics-free neighborhood of the point source when ρ and ν are analytic[17]. This assumption guarantees that the Hadamard-Babich ansatz remains valid in all cases considered. We refer the reader to [17, 27, 28] for a detailed account of how the Hadamard-Babich ansatz can be combined with the fast Huygens sweeping method to naturally handle caustics.

According to the essence of asymptotics[13], the difference between the true Green's function G and the HB ansatz G_B can be written as

$$G\left(\omega, \boldsymbol{x}_0; \boldsymbol{x}\right) - G_B\left(\omega, \boldsymbol{x}_0; \boldsymbol{x}\right) = O(1/\omega^{\infty}), \tag{4.8}$$

where the "error" term on the right-hand side means that the difference can be made arbitrarily smooth for all $\boldsymbol{x}$, as long as τ^2 and $v_s, s = 0, 1, 2, \cdots$ are analytic. According to [15], when the source term f is compactly supported, we have

$$||u_{true} - u_{HB}^N||_{L^\infty(\Omega)} \leq O\left((1/\omega)^{N+1-\frac{m-3}{2}}\right), \tag{4.9}$$

where u_{true} represents the solution obtained by (2.2) with G being the true Green's function and u_{HB}^N represents the solution obtained by using the N-term truncation of G_B as the Green's function. We remark that (4.9) provides the asymptotic error estimate for resolvent $R(\omega)$ when employing the truncated HB ansatz as the approximate Green's function in an inhomogeneous medium.

5. Numerical implementation

Here we present the numerical implementation of the proposed resolvent $R_\sigma(\omega)$. We begin by providing detailed definitions of the complex scaling and cutoff functions required for the gluing. Next, we briefly discuss high-order numerical schemes for the eikonal and transport equations, which yield the squared phase function τ^2 and the HB coefficients v_s. To avoid solving the eikonal and transport equations at every source point, we introduce multivariate Chebyshev interpolation to precompute and compress the required ingredients. Based on the HB ansatz, we discretize the resolvents $R_{\sigma,0}(\omega)$ and $R(\omega)$ and carefully address the diagonal singularity of the Green's function (namely, the kernel function of the resolvent operator).

5.1. Complex scaling and cutoff functions

We define the computational domain as $\Omega = [-a_1, a_1] \times \cdots \times [-a_m, a_m]$, with $a_i > 0, i = 1, 2, \cdots, m,$. To construct the complex scaling, we introduce the complex stretching of the coordinates defined as

$$\widetilde{x}_i\left(x_i\right) = x_i + \mathrm{i}\int_0^{x_i} \sigma_i(t)dt \tag{5.1}$$

for $i = 1, 2, \cdots, m$. Here we take σ_i

$$\sigma_i(t) = \sigma_i(-t), \quad \sigma_i(t) = 0 \text{ for } |t| \leq a_i, \quad \sigma_i(t) > 0 \text{ for } |t| > a_i, \tag{5.2}$$

with $a_i > 0, i = 1, 2, \cdots, m$. Regions with non-zero σ_i $(i = 1, 2, \cdots, m)$ are called the complex scaling/PML region. For definiteness, throughout this paper, we use the positive function σ_i $(i = 1, 2, \cdots, m)$ [6, 16, 18]

$$\sigma_i\left(x_i\right) = \begin{cases} \frac{2Sg_i^P}{g_i^P + (1-g_i)^P}, & a_i \leq x_i \leq a_i + T_i, \\ S, & x_i > a_i + T_i, \\ 0, & -a_i < x_i < a_i, \\ \sigma_i\left(-x_i\right), & x \leq -a_i, \end{cases} \tag{5.3}$$

where $T_i > 0$ denotes the thickness of the complex scaling region, P is a positive integer, and

$$g_i = \left(\frac{1}{2} - \frac{1}{P}\right)\bar{x}_i^3 + \frac{\bar{x}_i}{P} + \frac{1}{2}, \quad \bar{x}_i = \frac{x_i - \left(a_i + T_i\right)}{T_i}. \tag{5.4}$$

It can be seen that σ_i maps $\left[a_i, a_i + T_i\right]$ onto $[0, S]$ and its derivatives vanish at $x_i = \pm a_i$ up to order $P-1$. We introduce a smooth function $\phi_{[a,b]}(x) \in C^\infty(\mathbb{R})$, defined as follows:

$$\phi_{[a,b]}(x) = \begin{cases} 0, & x \le a \\ \eta\left(\frac{x-a}{b-a}\right), & a < x < b \\ 1, & x \ge b \end{cases}, \quad \text{where} \quad \eta(t) = \frac{e^{-1/t}}{e^{-1/t} + e^{-1/(1-t)}}. \tag{5.5}$$

Building on this, we define the cutoff functions $\chi_K, \chi_\infty, \tilde{\chi}_K$, and $\tilde{\chi}_\infty$. To be specific, we use $m = 2$, $\Omega = [-1, 1]^2$, $T_1 = T_2 = 0.2$, and $K = [-0.4, 0.4]^2$ as a representative example. Thus, these functions are

$$\chi_K = \phi_{[-0.78,-0.62]}(x) \times (1 - \phi_{[0.62,0.78]}(x)) \times \phi_{[-0.78,-0.62]}(y) \times (1 - \phi_{[0.62,0.78]}(y)), \tag{5.6}$$

$$\tilde{\chi}_K = \phi_{[-0.98,-0.82]}(x) \times (1 - \phi_{[0.82,0.98]}(x)) \times \phi_{[-0.98,-0.82]}(y) \times (1 - \phi_{[0.82,0.98]}(y)), \tag{5.7}$$

$$\chi_\infty = 1 - \phi_{[-0.78,-0.62]}(x) \times (1 - \phi_{[0.62,0.78]}(x)) \times \phi_{[-0.78,-0.62]}(y) \times (1 - \phi_{[0.62,0.78]}(y)), \tag{5.8}$$

$$\tilde{\chi}_\infty = 1 - \phi_{[-0.58,-0.42]}(x) \times (1 - \phi_{[0.42,0.58]}(x)) \times \phi_{[-0.58,-0.42]}(y) \times (1 - \phi_{[0.42,0.58]}(y)). \tag{5.9}$$

In Figure 2, we illustrate the four cutoff functions that will be used in this article.

5.2. Precomputation of phase and HB coefficients

The Hadamard-Babich ansatz is characterized by the phase function τ satisfying the eikonal equation (4.5) and the HB coefficients $v_s, s = 0, 1, \cdots$ satisfying the transport equations (4.6). The weakly coupled eikonal equation (4.5) and transport equations (4.6) with point-source conditions have been solved to high-order accuracy by using Lax-Friedrichs weighted essentially non-oscillatory (LxF-WENO) sweeping schemes as demonstrated in [25]. The high-order schemes in [25] have adopted essential ideas from many sources, including [21, 14, 10, 24, 11, 31, 30, 29, 9, 20, 17] and have been used in many applications. Consequently, we will adopt these schemes to our setting as well, and we omit details here.

However, for a given point source $\boldsymbol{x}_0$, constructing the HB ansatz by sequentially solving the eikonal and transport equations and then evaluating a volume integral to obtain the solution $R(\omega)f$ at $\boldsymbol{x}_0$ is clearly computationally expensive. As a basis for efficient numerical implementation, the N-term truncation of the HB ansatz, $G_B^N(\omega, \boldsymbol{x}_0; \boldsymbol{x})$, for N small, should be evaluated with a computational cost of $O(1)$ for any $\boldsymbol{x}_0, \boldsymbol{x} \in \Omega$.

Since we have assumed that τ^2 and $v_s, s = 0, 1, \cdots$ are analytic in Ω, we introduce the multivariate Chebyshev interpolation to reduce the computational cost. We take the 2-D case as an example. Letting $q(x, y, x_0, y_0)$ be a function that admits a low-rank representation where $\boldsymbol{x} = [x, y], \boldsymbol{x}_0 = [x_0, y_0] \in \Omega$, we consider the following analytical low-rank representation using Chebyshev interpolation,

$$q(x, y, x_0, y_0) \approx \sum_{i=1}^{n_i}\sum_{j=1}^{n_j}\sum_{k=1}^{n_k}\sum_{l=1}^{n_l} Q(i, j, k, l)\bar{T}_i(x)\bar{T}_j(y)\bar{T}_k(x_0)\bar{T}_l(y_0), \tag{5.10}$$

where n_i, n_j, n_k, and n_l are the orders of Chebyshev interpolation, Q is a 4-D tensor of size $n_i \times n_j \times n_k \times n_l$ that contains the spectral coefficients to be determined, and $\bar{T}_i$, $\bar{T}_j$, $\bar{T}_k$, and $\bar{T}_l$ represent the Chebyshev interpolants defined via translating the standard Chebyshev polynomials T_p defined on $[-1, 1]$ to the corresponding domain,

$$T_p(s) = \cos(p \arccos(s)), \qquad s \in [-1, 1]. \tag{5.11}$$

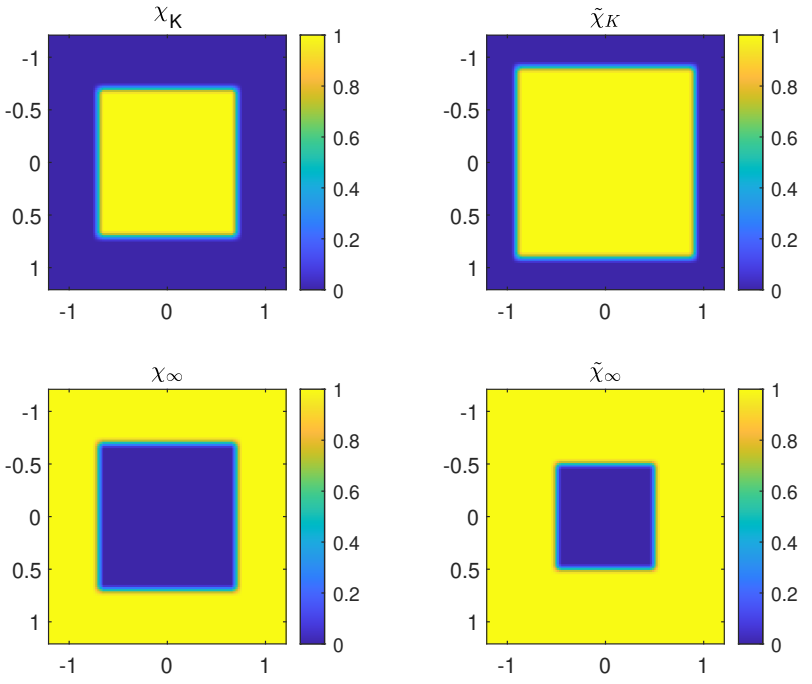

Figure 2: The cutoff functions used in the gluing procedure.

We can obtain Q by applying fast cosine transforms with respect to x, y, x_0, and y_0 to the tensor $q(x_i^c, y_j^c, x_{0,k}^c, y_{0,l}^c)$, where x_i^c, y_j^c, $x_{0,k}^c$, and $y_{0,l}^c$ are n_i, n_j, n_k, and n_l-order Chebyshev nodes in $\Omega\times\Omega$, respectively, which are also obtained by translating the n-order Chebyshev nodes $\{s_p\}$ in $[-1, 1]$,

$$s_p = \cos\left(\frac{2p-1}{2n}\right), \qquad p = 1, 2, \cdots, n. \tag{5.12}$$

Taking $q = \tau^2$ and v_s, $s = 0, 1, \cdots$, we now only need to evaluate them at the Chebyshev nodes, rather than on a fine grid satisfying the wave resolution requirement.

To calculate $q(x_i^c, y_j^c, x_{0,k}^c, y_{0,l}^c)$, we adopt a computational strategy as used in [15]: first choose a region Ω_c which is slightly larger than Ω, then compute numerically the ingredients in Ω_c with sources located at $[x_{0,k}^c, y_{0,l}^c]$, respectively, and finally use cubic spline interpolation of the just computed ingredients on uniform grids to obtain $q(x_i^c, y_j^c, x_{0,k}^c, y_{0,l}^c)$. Here Ω_c is introduced to ensure the accuracy of the interpolations near the boundary of Ω. And the weakly coupled eikonal and transport equations with point-source conditions can be solved to high-order accuracy by using Lax-Friedrichs weighted essentially non-oscillatory (LxF-WENO) sweeping schemes as demonstrated in [25].

Once the Chebyshev interpolation is constructed, we evaluate equation (5.10) to obtain the required ingredients and construct the resolvent by (5.14). We remark that the summation (5.10) can be accelerated by the Orszag partial summation method [5].

5.3. Discretization of the resolvents

In this subsection, we consider the numerical discretization of the resolvents $R(\omega)$ and $R_{\sigma,0}(\omega)$. We first discretize the domain Ω into N_v regular cells with cell size $h = O(1/\omega)$, with the cell centers denoted by $\{\boldsymbol{x}_i\}_{i=1}^{N_v}$.

Here we use the N-term truncation G_B^N as the asymptotic approximation. Then the resolvent $R(\omega)$ can be expressed as

$$[R(\omega)f](\boldsymbol{x}_0) \approx \int_\Omega G_B^N(\omega, \boldsymbol{x}_0; \boldsymbol{x}) f(\boldsymbol{x}) \mathrm{d}\boldsymbol{x} \tag{5.13}$$

To numerically compute (5.13), we then have

$$[R(\omega)f](\boldsymbol{x}_j) \approx \sum_{i=1}^{N_v} \frac{1}{h^m} K_{j,i} f(\boldsymbol{x}_i), \quad j = 1, 2 \cdots, N_v \tag{5.14}$$

where $K_{j,i} = G_B^N(\omega, \boldsymbol{x}_j; \boldsymbol{x}_i)$ for $i \neq j$ and the self-term $K_{i,i}$ can be computed analytically by integrating the free space Green's function over the source cell, assuming constant wave speed within each cell; see the appendix of [15] for details. Then the field values at cell centers, $u(\boldsymbol{x}_j)$, can be computed by matrix-vector multiplication

$$U = \frac{1}{h^m} K I_f, \tag{5.15}$$

where I_f denotes a vector of length N_v that collects $f(\boldsymbol{x}_i), i = 1, 2, \cdots, N_v$ and U denotes a vector that collects $u(\boldsymbol{x}_j), j = 1, 2, \cdots, N_v$.

The resolvent $R_{\sigma,0}$ differs slightly in that the wave field is defined over Ω_P, instead of Ω, correspondingly, the associated kernel matrix is not square. We discretize Ω_P into M_v regular cells with the same cell size h as used for Ω, and denote their centers by $\{\boldsymbol{y}_j\}_{j=1}^{M_v}$. Then we have

$$[R_{\sigma,0}(\omega)f](\boldsymbol{y}_j) = \int_\Omega \tilde{G}(\omega, \boldsymbol{y}_j; \boldsymbol{x}) f(\boldsymbol{x}) \mathrm{d}\boldsymbol{x} \approx \sum_{i=1}^{N_v} \frac{1}{h^m} \tilde{K}_{j,i} f(\boldsymbol{x}_i), \quad j = 1, 2 \cdots, M_v, \tag{5.16}$$

where $\tilde{K}_{j,i} = \tilde{G}(\omega, \boldsymbol{y}_j; \boldsymbol{x}_i)$ for $\boldsymbol{y}_j \neq \boldsymbol{x}_i$ and the self-term can likewise be computed analytically by integrating the free-space Green's function over the source cell. This is simpler because the medium is homogeneous in this case, and all self-term entries take the same value.

The explicit constructions of these kernel matrices and the matrix–vector multiplications incur computational cost of order $O(\omega^{2m})$, which is generally prohibitive. However, for high-frequency Helmholtz equations, we have developed efficient algorithms [19, 17, 15] based on hierarchical matrix representations and butterfly algorithms that reduce this cost to quasi-linear complexity for $m = 2$ and sub-quadratic for $m = 3$. Since our main goal here is to illustrate the feasibility of the new resolvent, at this stage we will not apply these advanced algorithms to compute the resolvent in this article. Instead, we will use two-dimensional numerical examples to demonstrate the convergence and performance of the proposed resolvent.

For the Laplace operator appearing in the commutator, we employ finite difference methods. We avoid FFT-based spectral methods here because the involved functions are truncated to the supports of gradients of cutoff functions, where spectral methods suffer from the Gibbs phenomena and the loss of accuracy.

6. Numerical examples

In this section, we first consider a homogeneous wave speed model, where the resolvents are known and can be used to generate exact reference solutions. In the subsequent examples, the reference solutions will be generated using the FDFD method. All numerical experiments were performed on a computer equipped with 512 GB of RAM and 56 CPU cores.

We will use the following source terms.

- $f_1 = \delta(x, y)$, where the solution corresponding to the source term f_1 is the Green's function.
- $f_2 = t(\sqrt{x^2 + y^2}, 0.1, 0.3)$, where $t(x, w_1, w_2)$ is the cosine tapering function:

$$t(x, w_1, w_2) = \begin{cases} 1, & x < w_1, \\ 0.5\left(1 + \cos\left(\pi(x - w_1)/(w_2 - w_1)\right)\right), & w_1 \le x \le w_2, \\ 0, & x > w_2. \end{cases} \tag{6.1}$$

- $f_3 = \exp(-(x^2 + y^2)/(2\sigma^2)) \sin(0.9\omega(x + y)) t(\sqrt{x^2 + y^2}, 0.1, 0.3)$, where $\sigma = 0.15$, and t is given by (6.1).

- $f_4 = \rho^{-1}\nabla\cdot(\nu\nabla u^{\text{inc}}(\boldsymbol{x})) + \omega^2 u^{\text{inc}}(\boldsymbol{x})$, where $u^{\text{inc}} = e^{\mathrm{i}\omega \boldsymbol{x}\cdot\boldsymbol{d}}$ is an incident plane wave, and $\boldsymbol{d}$ denotes the unit direction vector.

Here we mention in passing that the source term f_4 arises in the plane wave scattering problem in an inhomogeneous medium. The total wavefield $u^{\text{tot}} = u^{\text{inc}} + u^{\text{og}}$, where u^{og} is the scattered wavefield, is governed by

$$-\rho^{-1}\nabla\cdot(\nu\nabla u^{\text{tot}}(\boldsymbol{x})) - \omega^2 u^{\text{tot}}(\boldsymbol{x}) = 0. \tag{6.2}$$

Clearly, u^{og} satisfies

$$-\rho^{-1}\nabla\cdot(\nu\nabla u^{\text{og}}(\boldsymbol{x})) - \omega^2 u^{\text{og}}(\boldsymbol{x}) = \rho^{-1}\nabla\cdot(\nu\nabla u^{\text{inc}}(\boldsymbol{x})) + \omega^2 u^{\text{inc}}(\boldsymbol{x}). \tag{6.3}$$

Here, f_4 can serve as a compactly supported source term that generates the outgoing wavefield u^{og} as ρ and ν are equal to 1 outside K.

In the numerical examples, we will use the cutoff functions defined in formulas (5.6)-(5.9). We will use the leading term of the HB ansatz as the asymptotic Green's function, and employ the leading-term truncation of formula (3.3) to compute the resolvent R_σ:

$$\begin{aligned} u &= R_\sigma(\omega) f \\ &\approx F\left(I - A_K - A_\infty + A_K A_\infty\right) f. \end{aligned} \tag{6.4}$$

6.1. Constant model

We start with the constant model with

$$\rho(x,y) = \nu(x,y) = n(x,y) = 1, \quad (x,y) \in \Omega = [-1.2, 1.2]^2.$$

In this case, the exact (complex-scaled) resolvent is known to be $R_{\sigma,0}$. The phase function has an analytical formula $\tau(\boldsymbol{x}_0;\boldsymbol{x}) = |\boldsymbol{x}_0 - \boldsymbol{x}|$. The HB coefficients have analytical formulas $v_0(\boldsymbol{x}_0;\boldsymbol{x}) = \frac{1}{2\sqrt{\pi}}$ and $v_1(\boldsymbol{x}_0;\boldsymbol{x}) = 0$. Therefore, the HB ansatz becomes the exact Green's function $G_B(\omega,\boldsymbol{x}_0;\boldsymbol{x}) = \frac{\mathrm{i}}{4}H_0^1(\omega|\boldsymbol{x}_0 - \boldsymbol{x}|)$. We use high-order Lax-Friedrichs WENO methods with mesh size $h_0 = 0.01$ to solve the eikonal and transport equations with point sources, construct their low-rank representation with an order of $3\times3\times3\times3$ for Chebyshev interpolation, and compare the results with these exact formulas.

For the constant model, we consider $\omega = 10\pi$. The fields computed by the proposed method and related results are shown in Figure 3. Since the exact resolvent $R_{\sigma,0}$ is known in the homogeneous medium, we compare the resolvent computed by the proposed method with the exact one over the domain Ω_P, which includes the complex scaling region. Both the proposed resolvent and the exact one use a grid spacing of 0.02, which corresponds to 10 points per wavelength (PPW). In the left column of Figure 3, we consider the source $f = f_1$, which leads to the resolvent $R_{\sigma,0}$ itself. As shown in the second row, the resulting error is small in magnitude and is concentrated within the support of $\nabla\tilde{\chi}_K$, which is precisely the region where the two resolvents are glued together. This is expected, since in the second term of (3.6), we apply $R_{\sigma,0}$ to the equivalent source term $A_K f$, which is compactly supported within the support of $\nabla\tilde{\chi}_K$. In fact, finite-difference operations are restricted to this gluing region. In the third and fourth rows, we present the fields along $y = 0$ and $y = 0.6$, respectively. The two fields agree well, including within the complex scaling region, as expected given that the difference between them is already known to be small.

In the middle and right columns, we present the results corresponding to the source terms $f = f_2$ and $f = f_3$, respectively. In both cases, the errors relative to the exact solutions are very small. In a homogeneous medium, the HB ansatz does not introduce any asymptotic error, and the proposed method successfully achieves high accuracy for $R_{\sigma,0}$ as expected.

To illustrate the convergence of geometric series in (3.3), we denote

$$S_j(f) = (A_\infty A_K - A_\infty A_K A_\infty)^j f, \ j = 0, 1, \cdots \tag{6.5}$$

and present $S_j(f_3), j = 0, 1, \cdots, 5$ in Figure 4. The first term $S_0(f_3) = f_3$ is the source term, while the subsequent terms decay rapidly to zero due to the norm estimate of $A_\infty A_K$ given in (3.2). Therefore, a truncation after the first term is sufficient to approximate the resolvent via (3.6).

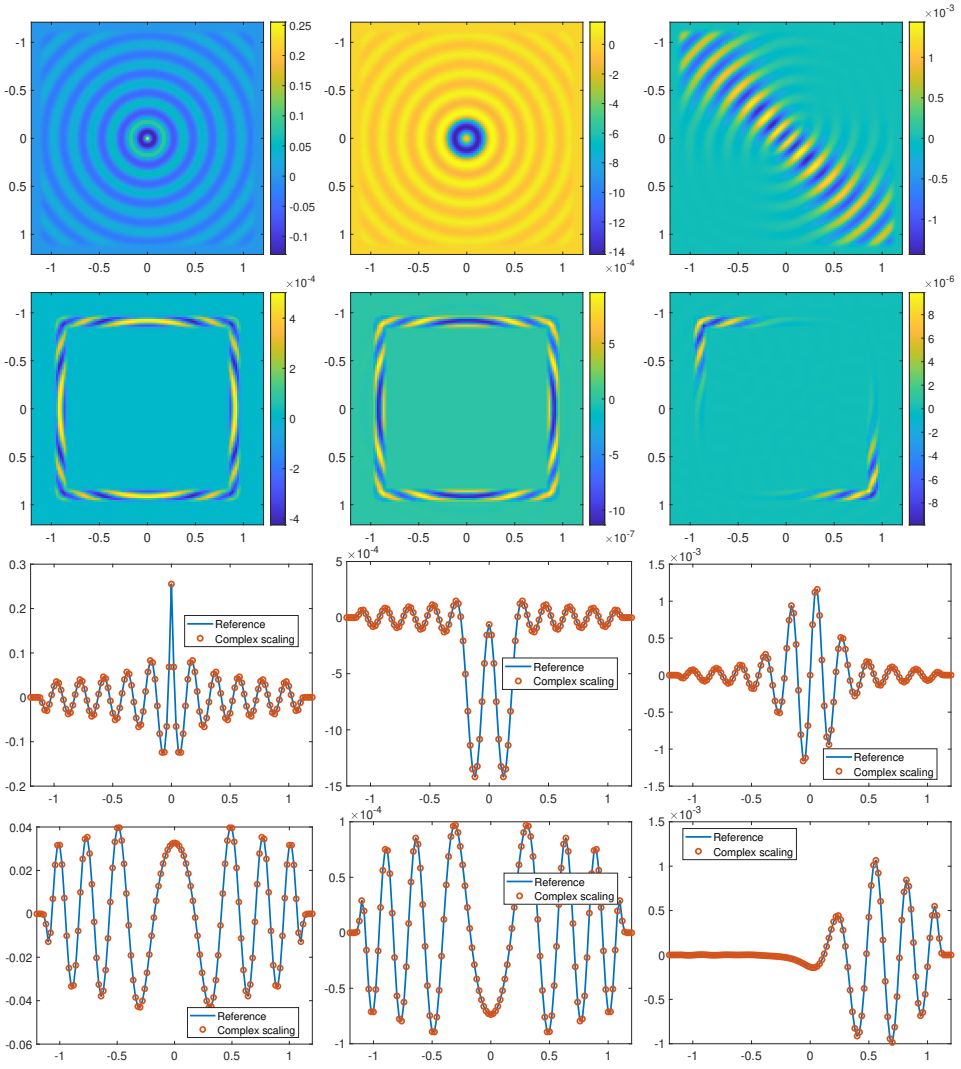

Figure 3: Constant model. $\omega = 10\pi$. Left column: source $f = f_1$. Middle column: source $f = f_2$. Right column: source $f = f_3$. Row 1: the field $\mathfrak{Re}(u)$ computed by the proposed method. Row 2: difference $\mathfrak{Re}(u - u_{\text{ref}})$, where the reference solution u_{ref} is obtained by the known resolvent $R_{\sigma,0}$. Row 3: the fields $\mathfrak{Re}(u)$(o) and $\mathfrak{Re}(u_{\text{ref}})$ (-) drawn along $y = 0$. Row 4: the fields $\mathfrak{Re}(u)$ and $\mathfrak{Re}(u_{\text{ref}})$ drawn along $y = 0.6$.

6.2. Gaussian model

Here we consider the Gaussian model with

$$\rho(x, y) = \frac{1}{\left(1 + 0.1\exp(-30(x^2 + y^2))\right)^2}, \quad \nu(x, y) = 1, \quad (x, y) \in \Omega = [-1.2, 1.2]^2.$$

We use high-order Lax-Friedrichs WENO methods with mesh size $h_0 = 0.01$ to solve the eikonal and transport equations with point sources, construct their low-rank representation with order $25 \times 25 \times 25 \times 25$ Chebyshev interpolation, and compare the results with the reference solution obtained by the FDFD method.

We consider $\omega = 10\pi$. The fields computed by the proposed method and related comparison results with the FDFD method are shown in Figure 5. In these comparisons, the proposed method still uses a grid spacing of 0.02 (corresponding to 10 points per wavelength, PPW = 10), while the FDFD method employs a finer grid spacing of 0.005 (PPW = 40) to reduce dispersion errors. The FDFD method provides reference solutions only within the computational domain Ω, excluding the complex scaling region.

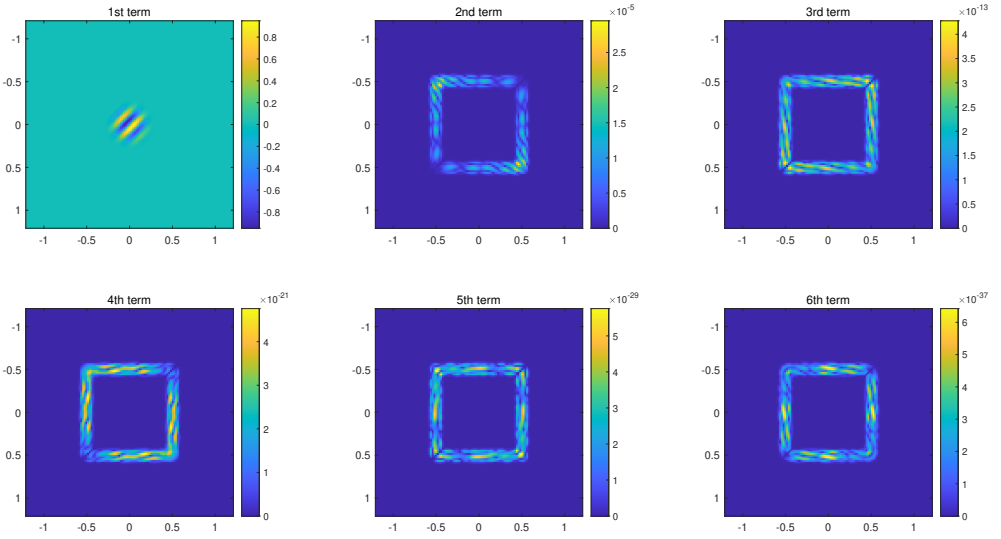

Figure 4: Constant model. $\omega = 10\pi$. The first six terms of the geometric series $\{S_j(f)\}$ for $f = f_3$.

In the left column of Figure 5, the source $f = f_1$ corresponds to the resolvent R_σ itself. We omit the reference solution at the point source location, where the solution is known to be singular. The proposed method yields the solution in an integral-averaged (weak) sense at this point. By comparing the wave field in the first row with the difference shown in the second row, we observe that the difference is small and uniform. The comparison in the third row is performed along the line $y = 0$, which passes through the point source at $[0, 0]$. Although the singular point itself is omitted, we observe that the two solutions agree very well in its vicinity, since the HB ansatz provides an asymptotic Green's function with uniform accuracy near the source.

In the middle and right columns, we present the results corresponding to the source terms $f = f_2$ and $f = f_3$, respectively. Unlike the case of a homogeneous medium, constructing $R(\omega)$ using the HB ansatz introduces asymptotic errors. To analyze the difference shown in the second row in Figure 5, we present in Figure 6 the difference between the fields computed by the proposed method and by the resolvent $R(\omega)$. Here, the reference solution in this case is also based on the HB ansatz, thereby eliminating the influence of the asymptotic error introduced by the HB ansatz. Consequently, the difference in Figure 6, arising from gluing together the two resolvents and the corresponding finite-difference operations, exhibits a behavior similar to that in the homogeneous medium case: it has a small magnitude and is concentrated within the support of $\nabla\tilde{\chi}_K$. Compared with the asymptotic error of the HB ansatz, which dominates the error shown in Figure 5, the error introduced by the gluing method proposed in this paper is negligible.

Due to the limitations of the reference solution, the comparison between the two fields is restricted to Ω. The results obtained by the proposed method match the reference solution well within Ω, and decay to zero in the complex scaling region $\Omega_P \setminus \Omega$. To investigate this rapid decay, Figure 7 plots the wave fields (in logarithmic scale) corresponding to the three source terms along the lines $y = 1.0, 1.1, 1.15$, and 1.2, respectively. A rapid decay to zero is observed as y approaches 1.2, consistent with the expected behavior of the complex scaling solution: it satisfies the original Helmholtz equation in Ω and decays rapidly in the complex scaling region $\Omega_P \setminus \Omega$.

To illustrate the convergence of geometric series in (3.3) within the inhomogeneous medium, we present $S_j(f_3)$, $j = 0, 1, \ldots, 5$, in Figure 8. We observe a similar rapid decay, since the norm estimate of $A_\infty A_K$ is derived based on the supports of the cutoff functions[8, (3.3)], which is independent of the homogeneity of the medium. Therefore, in an inhomogeneous medium, it is also sufficient to truncate after the first term and evaluate the resolvent using (3.6).

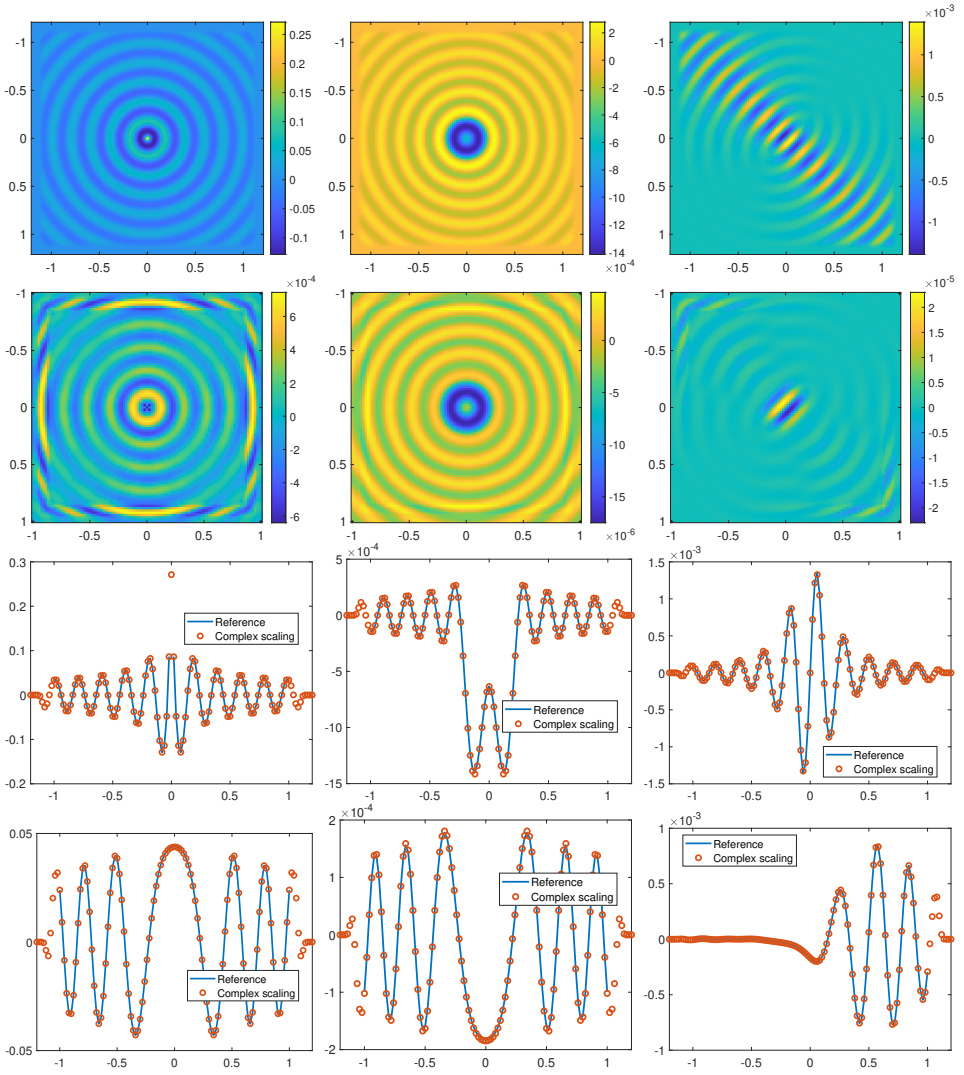

Figure 5: Gaussian model. $\omega = 10\pi$. Left column: source $f = f_1$. Middle column: source $f = f_2$. Right column: source $f = f_3$. Row 1: the field $\mathfrak{Re}(u)$ computed by the proposed method. Row 2: difference $\mathfrak{Re}(u - u_{\text{ref}})$, where the reference solution u_{ref} is obtained by the FDFD method. Row 3: the fields $\mathfrak{Re}(u)$ and $\mathfrak{Re}(u_{\text{ref}})$ drawn along $y = 0$. Row 4: the fields $\mathfrak{Re}(u)$ and $\mathfrak{Re}(u_{\text{ref}})$ drawn along $y = 0.6$.

6.3. Sinusoidal model

We consider the following medium

$$\rho(x, y) = \frac{1}{\big(1 + 0.3\exp(-30(x^2 + y^2))\sin(0.5\pi x)\cos(0.5\pi y + 0.1)\big)^2}, \quad \nu(x, y) = 1, \quad (x, y) \in \Omega = [-1.2, 1.2]^2.$$

We use high-order Lax-Friedrichs WENO methods with mesh size $h_0 = 0.01$ to solve the eikonal and transport equations with point sources, construct their low-rank representation with order $31 \times 31 \times 31 \times 31$ Chebyshev interpolation, and compare the results with the reference solution obtained by the FDFD method.

We consider $\omega = 10\pi$ and $\omega = 20\pi$ to investigate the accuracy and computational time of the proposed method at different frequencies, while keeping PPW = 10 fixed. For $\omega = 10\pi$, explicitly constructing the kernel matrices of the resolvents $R_{\sigma,0}$ and $R(\omega)$ takes 24.0 seconds, and the matrix-vector multiplication for each source term takes 0.8 seconds. For $\omega = 20\pi$, the kernel-matrix construction takes 141.6 seconds, and the matrix-vector multiplication takes approximately 13 seconds per source term. The computational time for matrix-vector multiplications scales as expected

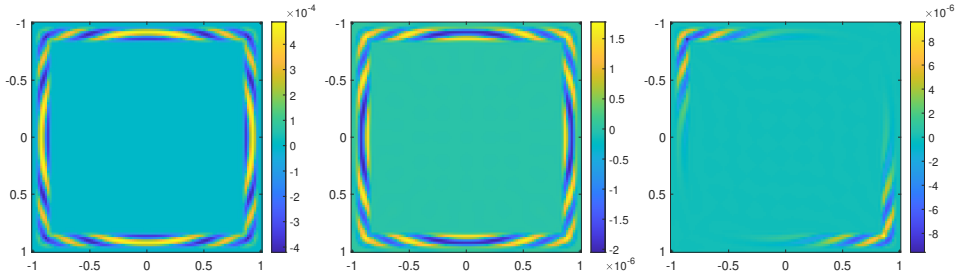

Figure 6: Gaussian model. $\omega = 10\pi$. Difference between the proposed complex-scaling resolvent R_σ and the original resolvent represented by the HB ansatz. Left: source $f = f_1$. Middle: source $f = f_2$. Right: source $f = f_3$.

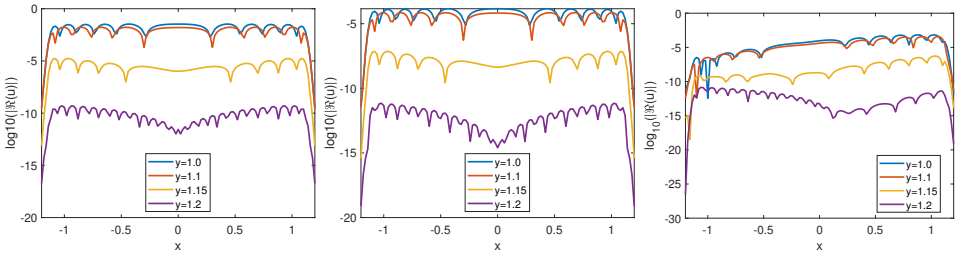

Figure 7: Gaussian model. $\omega = 10\pi$. $\mathfrak{Re}(u)$ along $y = 1.0,\ 1.1,\ 1.15,$ and 1.2 in log scale. Left: source $f = f_1$. Middle: source $f = f_2$. Right: source $f = f_3$.

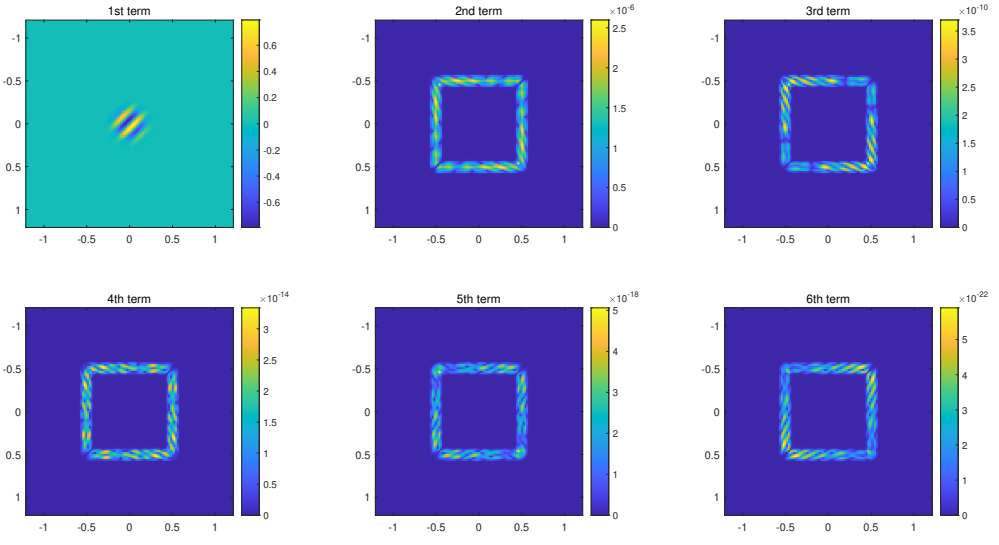

Figure 8: Gaussian model. $\omega = 10\pi$. The first six terms of the geometric series $\{S_j(f)\}$ for $f = f_3$.

with ω^4, while the time to construct kernel matrices increases more mildly due to the use of partial summation, which saves computational cost relative to direct summation as matrix size grows. In contrast, the FDFD method, maintaining PPW $= 40$, requires approximately 21.8 and 79.5 seconds to compute the wave field for each source term at $\omega = 10\pi$ and $\omega = 20\pi$, respectively.

Although the FDFD method appears to have shorter computational times, we emphasize two points: First, as the frequency increases, the FDFD method requires a corresponding increase in degrees of freedom in terms of points

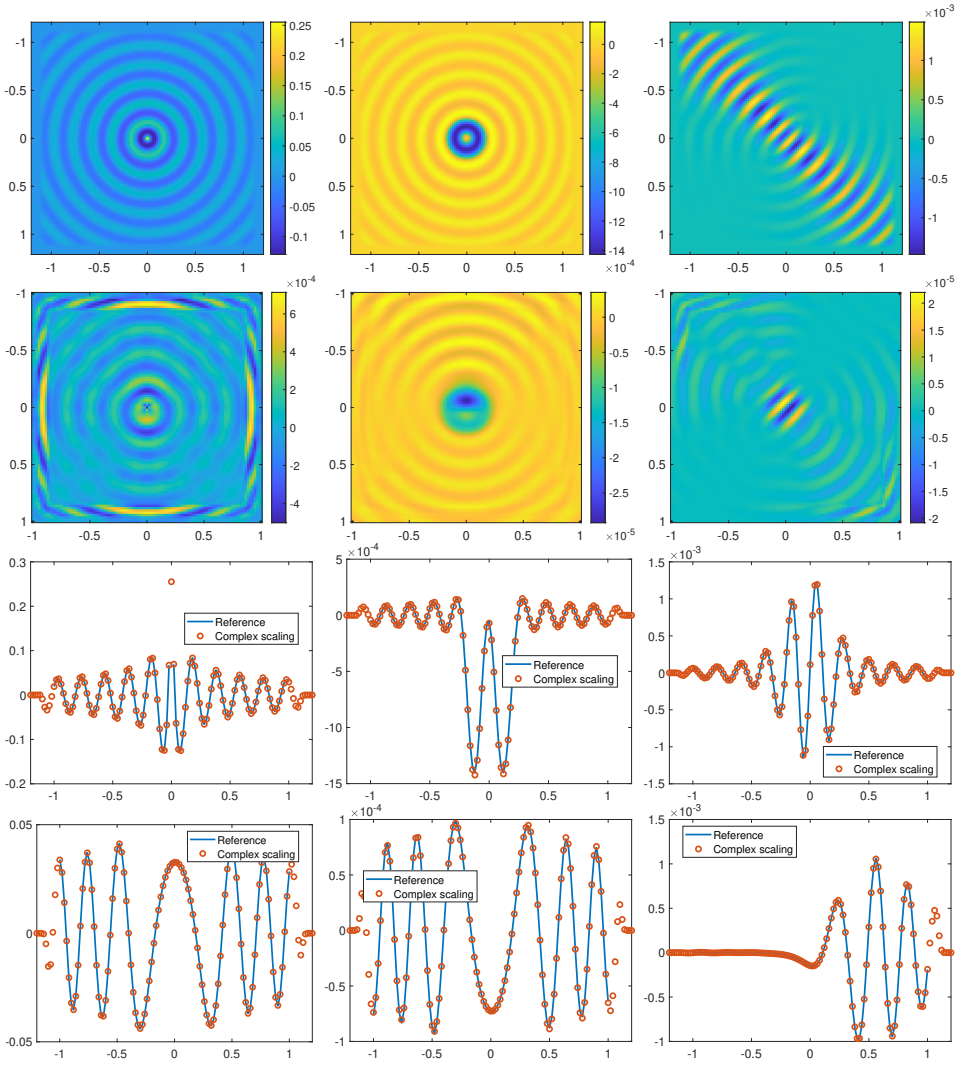

Figure 9: Sinusoidal model. $\omega = 10\pi$. Left column: source $f = f_1$. Middle column: source $f = f_2$. Right column: source $f = f_3$. Row 1: the field $\mathfrak{Re}(u)$ computed by the proposed method. Row 2: difference $\mathfrak{Re}(u - u_{\text{ref}})$, where the reference solution u_{ref} is obtained by the FDFD method. Row 3: the fields $\mathfrak{Re}(u)$ and $\mathfrak{Re}(u_{\text{ref}})$ drawn along $y = 0$. Row 4: the fields $\mathfrak{Re}(u)$ and $\mathfrak{Re}(u_{\text{ref}})$ drawn along $y = 0.6$.

per wavelength (PPW), resulting in nonlinear grid refinement, and there is no rigorous lower bound established for the scaling factor. This leads to a prohibitively high computational costs for high-frequency problems. Second, the resolvent we propose is implemented via oscillatory integral kernels, which do not introduce dispersion errors and thus require only linear grid refinement. Moreover, we have developed a series of hierarchical decomposition techniques based on the butterfly algorithm that significantly reduce the computational cost of such oscillatory integrals [19, 22, 23, 17, 27, 28, 15]. The integration of butterfly algorithms with the proposed resolvent computational framework constitutes a part of our ongoing research.

For $\omega = 10\pi$ and $\omega = 20\pi$, the fields computed by the proposed method along with the comparison results with the FDFD method are presented in Figures 9 and 10.

Finally, we consider a plane wave scattering problem with the source term f_4, where $\boldsymbol{d} = [-\sqrt{2}/2, -\sqrt{2}/2]$. Even though u^{tot} is not outgoing, the scattered wave u^{og} is and can therefore be effectively absorbed by the complex scaling layer. We show the scattered fields u^{og} at frequencies 10π and 20π computed by the proposed method in Figure 11, where the PPW is set to 10 in both cases. The results are compared with the reference solutions generated by the

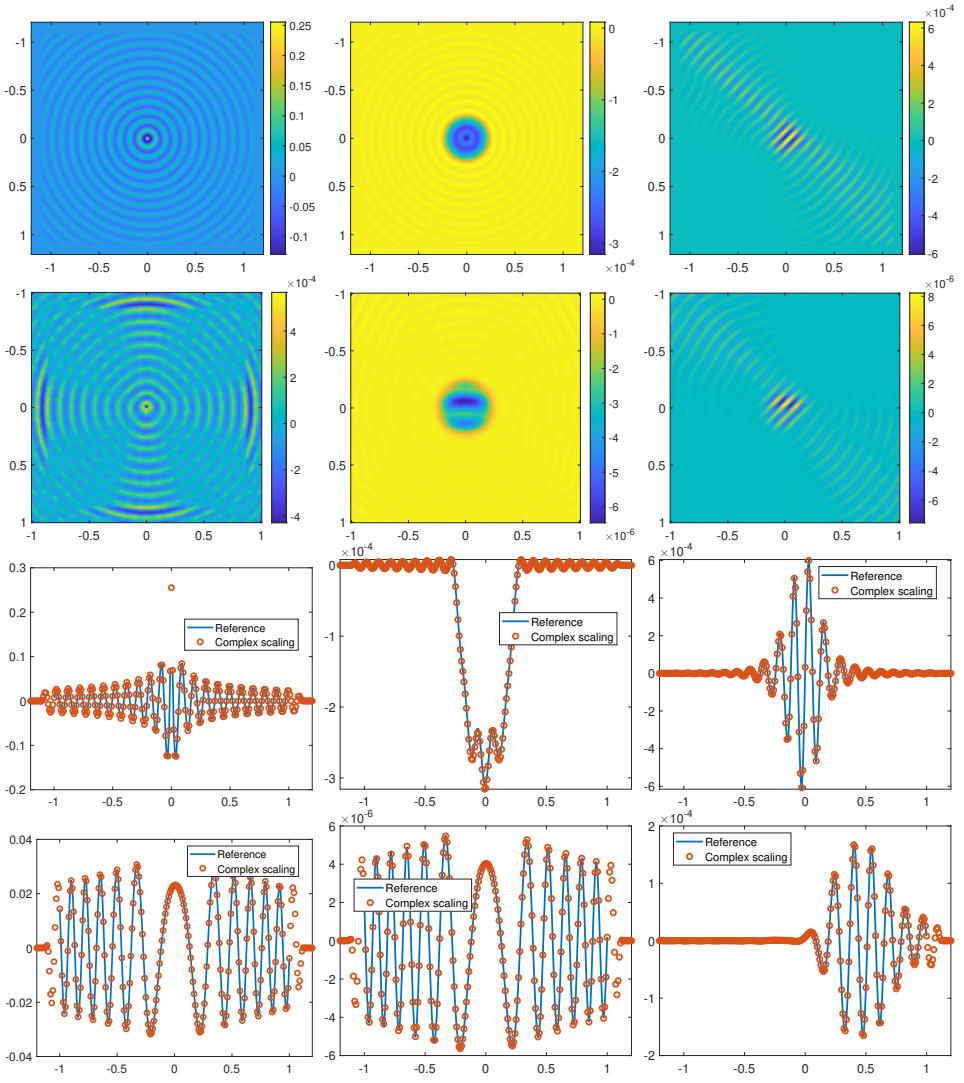

Figure 10: Sinusoidal model. $\omega = 20\pi$. Left column: source $f = f_1$. Middle column: source $f = f_2$. Right column: source $f = f_3$. Row 1: the field $\mathfrak{Re}(u)$ computed by the proposed method. Row 2: difference $\mathfrak{Re}(u - u_{\text{ref}})$, where the reference solution u_{ref} is obtained by the FDFD method. Row 3: the fields $\mathfrak{Re}(u)$ and $\mathfrak{Re}(u_{\text{ref}})$ drawn along $y = 0$. Row 4: the fields $\mathfrak{Re}(u)$ and $\mathfrak{Re}(u_{\text{ref}})$ drawn along $y = 0.6$.

FDFD method with PPW = 40. The complex scaling solutions agree well with the reference solutions within the computational domain and decay rapidly inside the complex scaling region. This indicates that the proposed resolvent can be effectively applied to scattering problems.

The numerical results confirm that the complex scaling solutions obtained by the proposed method exhibit the following properties:

- They satisfy the original Helmholtz equation within the computational domain;
- They exhibit rapid decay in the complex scaling region.

7. Conclusion

In this paper, we propose an explicit representation of the complex scaled resolvent operator associated with the Helmholtz equation in an inhomogeneous medium, which may have potential applications in scattering problems. By

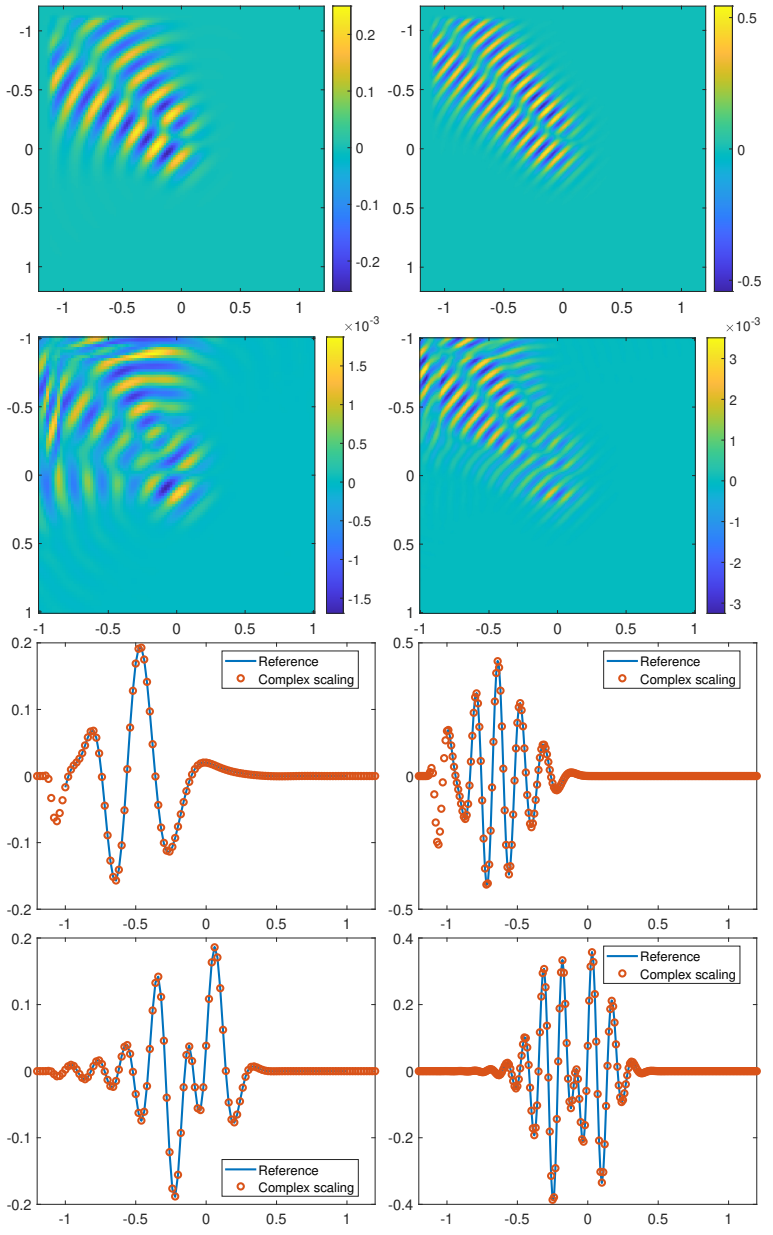

Figure 11: Sinusoidal medium. $f = f_4$ with $\boldsymbol{d} = [-\sqrt{2}/2, \sqrt{2}/2]$. Left column: $\omega = 10\pi$. Right column: $\omega = 20\pi$. Row 1: the scattered wavefield $\mathfrak{Re}(u^{\text{og}})$ computed by the proposed method. Row 2: difference $\mathfrak{Re}(u^{\text{og}} - u^{\text{og}}_{\text{ref}})$. Row 3: the fields $\mathfrak{Re}(u^{\text{og}})$ and $\mathfrak{Re}(u^{\text{og}}_{\text{ref}})$ drawn along $y = -0.9$. Row 4: the fields $\mathfrak{Re}(u^{\text{og}})$ and $\mathfrak{Re}(u^{\text{og}}_{\text{ref}})$ drawn along $y = 0$.

gluing together the non-complex-scaled resolvent in an inhomogeneous medium and the complex-scaled resolventin a homogeneous medium, we obtain the desired resolvent expressed as a geometric series. The former admits an asymptotic representation via the Hadamard–Babich ansatz, while the latter admits an explicit expression via analytic continuation. Numerical experiments are presented to demonstrate that the proposed resolvent can yield highly accurate solutions for the complex scaling method on relatively coarse grids, which satisfy the Helmholtz equation in the computational domain and decay rapidly within the complex scaling region. The integration of butterfly algorithms with the proposed complex-scaling resolvent computational framework forms a part of our ongoing work.

Acknowledgment

Kiril Datchev was partially supported by a Simons collaboration grant for mathematicians, and is grateful to Maciej Zworski for helpful discussions and suggestions. Shingyu Leung was partially supported by the Hong Kong RGC grants 16302223 and 16300524. Jianliang Qian was partially supported by NSF grants 2152011 and 2309534 and an MSU SPG grant.

References

[1] V. M. Babich. The short wave asymptotic form of the solution for the problem of a point source in an inhomogeneous medium. *USSR Computational Mathematics and Mathematical Physics*, 5(5):247–251, 1965.

[2] I. M. Babuška and S. A. Sauter. Is the pollution effect of the FEM avoidable for the Helmholtz equation considering high wave numbers? *SIAM Review*, 42:451–484, 2000.

[3] A. Bayliss, C. I. Goldstein, and E. Turkel. On accuracy conditions for the numerical computation of waves. *J. Comput. Phys.*, 59:396–404, 1985.

[4] J.-P. Berenger. A perfectly matched layer for the absorption of electromagnetic waves. *J. Comput. Phys.*, 114:185–200, 1994.

[5] J. P. Boyd. *Chebyshev and Fourier Spectral Methods*. Second edition, Dover, New York, 2001.

[6] D. Colton and R. Kress. *Inverse acoustic and electromagnetic scattering theory*. Springer, Berlin, 1998.

[7] K. Datchev and A. Vasy. Gluing semiclassical resolvent estimates via propagation of singularities. *International Mathematics Research Notices*, 2012(23):5409–5443, 2012.

[8] S. Dyatlov and M. Zworski. *Mathematical theory of scattering resonances*, volume 200. American Mathematical Soc., 2019.

[9] S. Fomel, S. Luo, and H. K. Zhao. Fast sweeping method for the factored eikonal equation. *J. Comput. Phys.*, 228:6440–6455, 2009.

[10] G. S. Jiang and D. Peng. Weighted ENO schemes for Hamilton-Jacobi equations. *SIAM J. Sci. Comput.*, 21:2126–2143, 2000.

[11] C. Y. Kao, S. J. Osher, and J. Qian. Lax-Friedrichs sweeping schemes for static Hamilton-Jacobi equations. *J. Comput. Phys.*, 196:367–391, 2004.

[12] M. Lassas and E. Somersalo. Analysis of the pml equations in general convex geometry. *Proc. R. Soc. Edinburgh Sect. A Math.*, 131(5):1183–1207, 2001.

[13] P. Lax. Asymptotic solutions of oscillatory initial value problems. *Duke Math. J.*, 24:627–645, 1957.

[14] X. D. Liu, S. J. Osher, and T. Chan. Weighted Essentially NonOscillatory schemes. *J. Comput. Phys.*, 115:200–212, 1994.

[15] Y. Liu, J. Song, R. Burridge, and J. Qian. A fast butterfly-compressed Hadamard-Babich integrator for high-frequency Helmholtz equations in inhomogeneous media with arbitrary sources. *SIAM Multiscale Model. Simul.*, 21:269–308, 2023.

[16] W. Lu, Y. Lu, and J. Qian. Perfectly-matched-layer boundary integral equation method for wave scattering in a layered medium. *SIAM J. Applied Math.*, 78:246–265, 2018.

[17] W. Lu, J. Qian, and R. Burridge. Babich's expansion and the fast Huygens sweeping method for the Helmholtz wave equation at high frequencies. *J. Comput. Phys.*, 313:478–510, 2016.

[18] W. Lu, L. Xu, T. Yin, and L. Zhang. A highly accurate perfectly-matched-layer boundary integral equation solver for acoustic layered-medium problems. *SIAM J. Sci. Comput.*, 45(4):B523–B543, 2023.

[19] S. Luo, J. Qian, and R. Burridge. Fast Huygens sweeping methods for Helmholtz equations in inhomogeneous media in the high frequency regime. *J. Comput. Phys.*, 270:378–401, 2014.

[20] S. Luo, J. Qian, and R. Burridge. High-order factorization based high-order hybrid fast sweeping methods for point-source eikonal equations. *SIAM J. Numer. Analy.*, 52:23–44, 2014.

[21] S. J. Osher and C. W. Shu. High-order Essentially NonOscillatory schemes for Hamilton-Jacobi equations. *SIAM J. Numer. Analy.*, 28:907–922, 1991.

[22] J. Qian, J. Song, W. Lu, and R. Burridge. Hadamard-Babich ansatz for point-source elastic wave equations in variable media at high frequencies. *SIAM Multiscale Model. Simul.*, 19:46–86, 2021.

[23] J. Qian, J. Song, W. Lu, and R. Burridge. Truncated Hadamard-Babich ansatz and fast Huygens sweeping methods for time-harmonic high-frequency elastic wave equations in inhomogeneous media. *Minimax Theory and its Applications*, 8:171–212, 2023.

[24] J. Qian and W. W. Symes. An adaptive finite difference method for traveltime and amplitude. *Geophysics*, 67:167–176, 2002.

[25] J. Qian, L. Yuan, Y. Liu, S. Luo, and R. Burridge. Babich's expansion and high-order Eulerian asymptotics for point-source Helmholtz equations. *J. Sci. Comput.*, 67:883–908, 2016.

[26] J. Sjöstrand and M. Zworski. Complex scaling and the distribution of scattering poles. *J. Amer. Math. Soc.*, 4(4):729–769, 1991.

[27] Y. Wei, J. Cheng, R. Burridge, and J. Qian. Hadamard integrator for time-dependent wave equations: Lagrangian formulation via ray tracing. *J. Comput. Phys.*, 497:112637, 2024.

[28] Y. Wei, J. Cheng, S. Leung, R. Burridge, and J. Qian. Hadamard integrators for wave equations in time and frequency domain: Eulerian formulations via butterfly algorithms. *J. Sci. Comput.*, 100(3):79, 2024.

[29] L. Zhang, J. W. Rector, and G. M. Hoversten. Eikonal solver in the celerity domain. *Geophys. J. Internat.*, 162:1–8, 2005.

[30] Y. T. Zhang, H. K. Zhao, and J. Qian. High order fast sweeping methods for static Hamilton-Jacobi equations. *J. Sci. Comp.*, 29:25–56, 2006.

[31] H. K. Zhao. Fast sweeping method for eikonal equations. *Math. Comp.*, 74:603–627, 2005.